Hot spots in superconducting tantalum

A. Hahn, S. Hofmann, K. Hümpfner, and M. Schatz
Institut für Werkstoffe der Elektrotechnik, Ruhr-Universität D44780 Bochum, Germany
(Received 26 June 2001; revised manuscript received 8 January 2002; published 28 May 2002)

We discuss experimental results on nonequilibrium superconductivity in Ag-Ta point contacts. From a hysteretic dc characteristics we conclude a normal bubble suddenly to form in the superconductor below the contact at a critical bias, its radius $R(U)$ monotonically increasing with bias voltage U. The observed radii are unexpectedly large compared with what is expected from existing models. The investigation is intended to describe this behavior in physical terms and theoretically to calculate the function $R(U)$ for varying values of contact resistance. We calculate mean values over the bubble volume of the electron and phonon distribution functions using simplified Boltzmann equations which describe the effects of electron injection into the bubble, electron-phonon scattering, and electron and phonon escape from the bubble to the surrounding superconductor. Downscattering of high-energy injected quasiparticles into subgap states $0<E<\Delta$ leads to strong occupation of subgap states because escape is prevented for these energies by Andreev reflection from the N-S interface. This explains the large bubble size. In contrast with this, occupation of states $E>\Delta$ is typically two orders of magnitude smaller. The function $R(U)$ is determined by a self-consistency condition postulating that the calculated nonequilibrium distribution function $f(E)$ satisfies the BCS gap equation in the limit of vanishing gap parameter. Agreement of the calculated and the experimentally determined $R(U)$ functions is satisfactory.

DOI: 10.1103/PhysRevB.65.224503 PACS number(s): 74.80.Fp, 74.40.+k

I. INTRODUCTION

Geometrical resonances of electronic quasiparticle waves on normal-metal–superconductor (N/S) and S/N/S sandwich structures have found much interest for nearly 40 years.[1–3] Perhaps, Tomasch oscillations[2] represent the best-known example for the corresponding phenomena. More recently, also more complex geometrical structures have found attention, e.g., one-dimensional superlattices composed of periodically alternating N and S layers.[4–6] Moreover, strong-coupling effects were taken into account[7] or application was made to high-temperature superconductors.[8] In all of these cases the geometry was fixed by chemical composition or crystallographic structure. In contrast with this, our group has reported[9,10] resonance phenomena on a nonequilibrium structure in a chemically and crystallographically homogeneous material, tantalum. The spatial structure was generated by injecting across an Ag/Ta point contact an electrical current strong enough to destroy superconductivity in a certain region called the normal bubble in what follows. The extent of this N region is not fixed but is variable in this case, the bubble growing with increasing current, thus leading to new aspects of the resonance phenomena observed.

As far as we are aware, similar observations of, say, quasiparticle interference effects on hot spots have not been observed by other authors despite an appreciable amount of literature on self-heating effects in weak links and similar structures; see, e.g., the reviews by Gurewich and Mints[11] and by Gross and Koelle.[12]

The interference phenomena under question manifest themselves by a fine structure on a high-current branch of the current-voltage characteristics which is separated from a low-current branch by a hysteretic transition. Measuring along that branch the voltage dependence of the differential conductance $G(U)=dI/dU$ one observes a series of anharmonic oscillations[9,10] with amplitudes strongly decreasing with voltage U. In particular, the series of minima in $G(U)$ is rather pronounced with up to four periods observable. Examples may be found in previous papers quoted above and some more will be given in Sec. II.

We interpret these structures as interference phenomena of quasiparticle waves on the geometry of the bubble, the characteristic quasiparticle energy E involved being the gap energy Δ. We assume, as the most natural assumption, a half-sphere shape of the bubble centered around the injection orifice[13] (see Fig. 2 below). Let $R=R(U)$ denote the radius of the bubble (increasing with voltage U); then, independent of the particular mechanism by which the current-voltage characteristics is influenced by the interference phenomenon, the observed periodicity must correspond to the radii

$$R=R_n=n\cdot\xi', \tag{1}$$

with

$$\xi'=\pi^2\xi_0/2 \quad \text{and} \quad \xi_0=\hbar v_F/(\pi\Delta)=92.5 \text{ nm} \tag{2}$$

the coherence length of tantalum. $n=1,2,\ldots$ is the interference order.

Equation (1) is the condition of constructive interference of $(E=\Delta)$ quasiparticles Andreev reflected[14] at the N/S phase boundary and normally reflected at the surface.

The importance of the radii given by (1) was emphasized by Gunsenheimer and one of the authors[15] who investigated the quasiparticle spectrum of a normal (full-)sphere imbedded in the (infinitely extended) superconductor. Their results may be re-interpreted in terms of the half-sphere model of Fig. 2 which (specular normal reflection at the surface assumed) yields the same results.[16] Their particular interest was in the subgap $(E<\Delta)$ states which are expected highly occupied by nonequilibrium scattering processes. Not unexpectedly, they find characteristic peculiarities just for the radii given by Eq. (1). Without being able to give a satisfactory

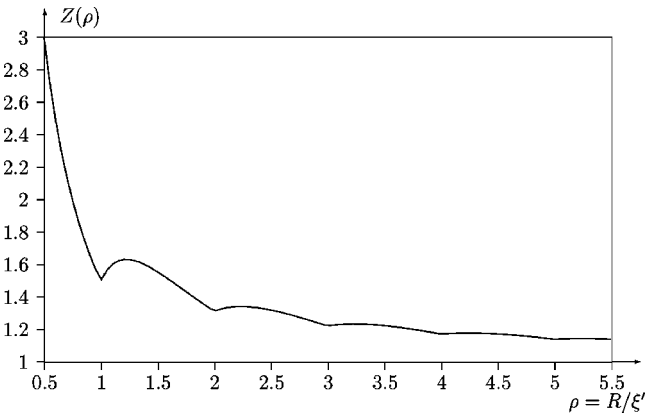

FIG. 1. For a normal sphere in an infinitely extended superconductor or a normal half-sphere according to Fig. 2: normalized number of subgap states vs radius. Radius in units of the characteristic length defined in Eq. (2).

theory of the current-voltage characteristics they argue that these peculiarities must be reflected in the characteristics at the set of voltages for which $R(U)$ equals the characteristic values given by Eq. (1). Some quantitative idea of their results on the subgap spectrum is supplied by Fig. 1 which displays, as a function of

$$R/\xi' = \rho, \tag{3}$$

the quantity $Z(\rho)$ defined as the total number of subgap states divided by $(2\pi/3)R^3 \times 2N_0\Delta$. Here N_0 is the (one spin) density of states per unit volume. Hence $2N_0\Delta$ is the number of subgap states per unit volume in the bulk limit $R \to \infty$. $Z(\rho)$ is given by

$$Z(\rho) = \frac{3}{2}\frac{n(\rho)+1}{\rho} - \frac{1}{4}\frac{n(\rho)[n(\rho)+1][2n(\rho)+1]}{\rho^3}, \tag{4}$$

with $n(\rho) = \mathrm{trunc}(\rho)$ the largest integer smaller than ρ. Equation (4) may easily be derived from Eq. (3) of Ref. 15.

Inspection of Fig. 1 illustrates what was stated above: The subgap spectrum is characterized by peculiarities repeating at integer values of $\rho = R/\xi'$. In particular, $Z(\rho)$ shows a discontinuous first derivative just at integer values of ρ.

We emphasize here that despite some attempts[9,10] a satisfactory theory of the current-voltage characteristics does not exist. The problem is addressed in Ref. 15. Nevertheless, attributing the structures in $G(U)$ to integer values of R/ξ' and thus measuring $R(U)$ is safely founded due to the simplicity and generality of Eq. (1). We have measured the bubble size as a function of voltage bias using Eq. (1). Some of these results[9,10] and additional unpublished ones will be presented as experimentally determined $R(U)$ relations in Sec. II. However, there is no physical discussion of $R(U)$ up to now. Such a discussion is the main aim of the present investigation which intends theoretically to explain the observed $R(U)$ behavior, say the rule of growing of the bubble.

At first sight, the results on $R(U)$ were unexpected. In particular, they contrasted with the predictions of Tinkham, Octavio, and Skocpol[17] and Tinkham[18] proposed for strong

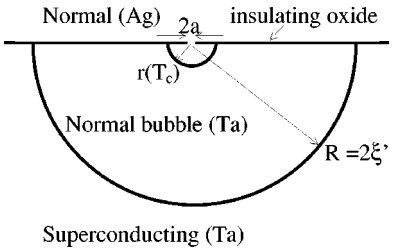

FIG. 2. Ag/Ta point contact produced by short circuiting a high resistance tunneling junction. Typical length scales for $R_N = 0.29\ \Omega$, $U = 9.1$ mV: orifice diameter $2a$, bubble size $r(T_c)$ expected according to Ref. 17, and observed bubble size $R = 2\xi'$, represented true to scale.

three-dimensional cooling in terms of the ''intersecting cone model.'' This model should have been relevant for our situation allowing us to calculate the temperature $T(r)$ in its dependence on distance r from the contact. Combining Eqs. (16) and (12) of Ref. 17 we obtain under reasonable assumptions concerning our contacts[19]

$$T^2(r) - T_B^2 = \frac{6}{\pi^4}\frac{e^2}{k^2}U^2\frac{a^2}{r^2}\left(1 - \frac{4a^2}{\pi^2 r^2}\right) \tag{5}$$

and

$$R_N = \frac{\pi}{16}\frac{\rho_0 l}{a^2}. \tag{6}$$

Here T_B is the bath temperature, e and k are the electronic charge and Boltzmann constant, respectively, a is the radius of the injection orifice, R_N is the contact resistance in the normal state, and

$$\rho_0 l = \frac{3}{2e^2 v_F N_0} = 9 \times 10^{-16}\ \Omega\,\mathrm{m}^2 \tag{7}$$

is the (l-independent) product of resistivity and mean free path. The numerical value given on the right-hand side of Eq. (7) results from the data which will be given in Sec. IV A.

For $T_B = 1.4$ K we obtain from the above equations for a typical contact with $R_N = 0.29\ \Omega$ at a voltage $U = 9.1$ mV an orifice radius $a = 24.7$ nm and a temperature equal to the critical temperature $T_c = 4.5$ K at a distance $r(T_c) = 152$ nm. This value should set the scale for the bubble size.

Figure 2 illustrates the situation with the orifice diameter $2a$ and the expected bubble radius $r(T_c)$ represented true to scale. In fact, however, we observe for the above-given values of R_N and U the second resonance minimum. The bubble radius thus is $R = 2\xi' = 913$ nm or 6 times larger than expected, indicating that the model of Tinkham *et al.* is inapplicable.

In the present investigation we shall give a quantitative explanation of the giant bubble sizes observed. The idea is that escape of subgap quasiparticles from the bubble is prevented by Andreev reflection from the N/S phase boundary. As a consequence, excitation of subgap states is high enough

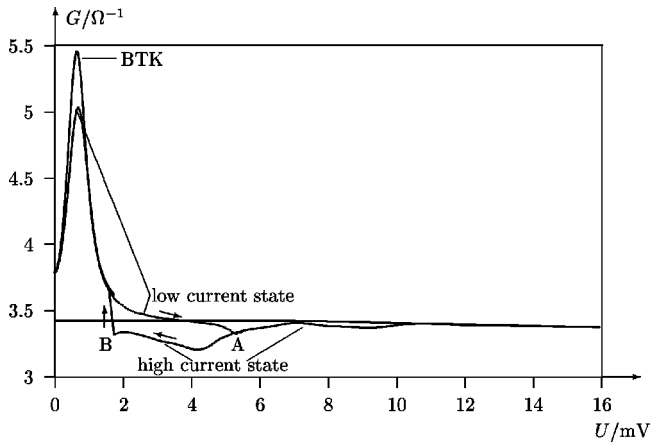

FIG. 3. Differential conductance versus voltage for a low-resistance contact ($R_N = 0.29\ \Omega$). Experimental curves labeled ''low-'' and ''high-current'' state. Nearly horizontal line: normal state. ''BTK'': Standard theory according to Ref. 22. ''BTK parameter'' $Z = 0.536$.

to destroy superconductivity in a large volume. A corresponding model is developed in Sec. III and its results are compared with the experiments in Sec. V after a review, given in Sec. IV, of independent electronic and phononic data for tantalum entering the theory. A final discussion is given in Sec. VI. First of all, however the experimental results are given in Sec. II.

II. EXPERIMENTAL RESULTS

Some experimental results were previously given.[9,10] Additional material is contained in unpublished work[20] from which the raw data were taken which finally lead to Figs. 5 and 6 below. Concerning sample preparation and characterization we refer to previous papers[9,10] and here only summarize as follows.

All experimental results refer to N/S point contacts with the superconductor S being high-purity tantalum prepared as a molten droplet under ultra high-vacuum conditions.

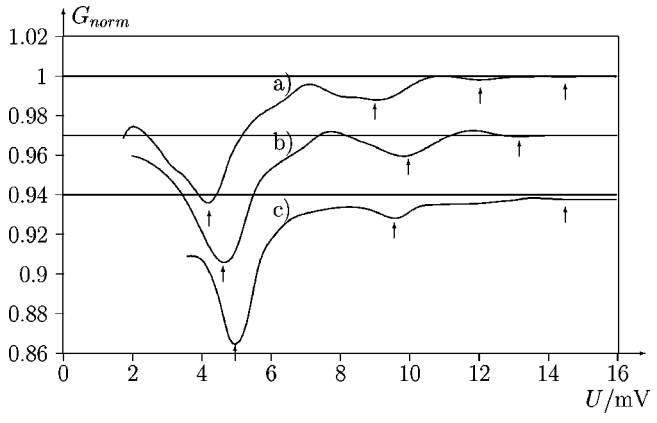

FIG. 4. Differential conductance of three low-resistance contacts normalized to the normal-state conductance. $R_N/\Omega = 0.292$ for sample (a), 0.291 for (b), and 0.383 for (c), respectively. Minima indicated by arrows. Ordinate scale attributed to curve (a). Curves (b) and (c) shifted vertically by -0.03 and -0.06, respectively.

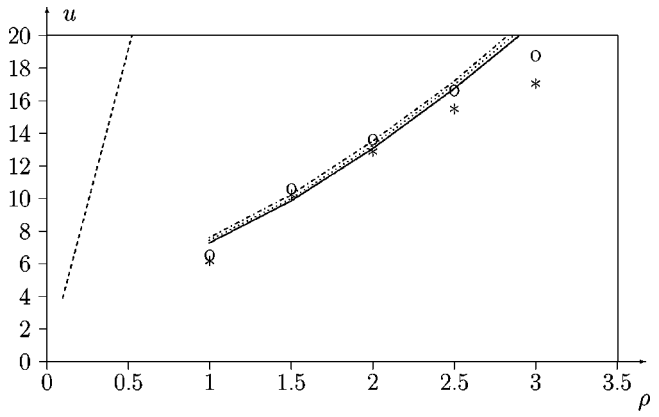

FIG. 5. For samples (a) (*) and (b) (o): Positions on voltage scale of minima and maxima in Fig. 4 are attributed to integer and half-integer values of $\rho = R/\xi'$. Dashed line represents the expectation according to Ref. 17. Solid, dotted, and dash-dotted curves are results of the model to be presented and will be discussed in Sec. V

Residual resistivity ratios of the Ta electrode were measured by an eddy current method. They exceeded 5000 in each case, indicating an elastic mean free path larger than 50 μm and thus large compared with all physically relevant lengths including the maximum observed radius $R = 3\xi'$ of the nonequilibrium bubble.

The N electrode was evaporated silver. The point contact resulted from electrically short circuiting a high-resistance $Ta/Ta_2O_5/Ag$ tunneling junction. The resistance of the resulting metallic point contact was typically between 0.2 and 1.5 Ω.

All measurements were performed at a bath temperature $T_B = 1.4$ K.

A typical trace of the differential conductance $G = dI/dU$ vs voltage U characteristics is shown by two curves in Fig. 3 labeled ''low-'' and ''high-current'' states, respectively. With bias increasing from zero, the low-current state persists up to point A where a discontinuous transition occurs to the high-current state indicated by a drastic decrease of the

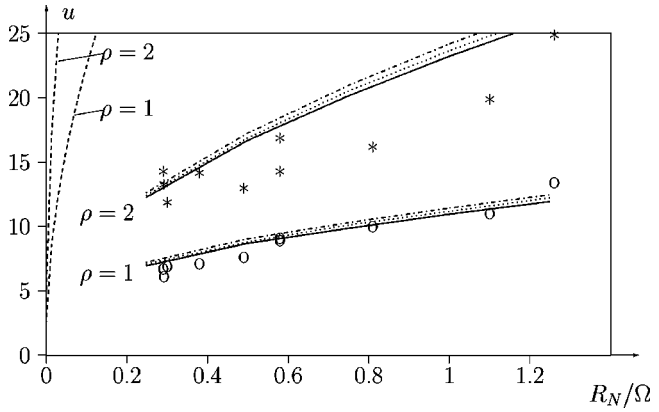

FIG. 6. Voltage of first (o) and second (*) minimum in $G(U)$ vs contact resistance R_N. Dashed curves: expectation according to Ref. 17. Solid, dotted, and dash-dotted curves are results of the model to be presented and will be discussed in Sec. V

excess current.[21] After exceeding point *A* and then again decreasing bias the lower curve is traced down to point *B*, the system remaining in the high-current state. Within each state, low or high current, respectively, the characteristics is perfectly reversible. In particular, in the high-current state all points of the lowermost curve in Fig. 3 down to point *B* are perfectly reproduced with increasing as well as decreasing bias. At point *B* the system jumps back to the low-current state.

In the low-current state the characteristics approximately follow the standard [Blonder-Tinkham-Klapwijk (BTK)] theory[22] with some deviations which at least for higher bias (approaching point *A* from below) must be due to heating effects. The corresponding theoretical curve is represented as ''BTK'' in the diagram. It was calculated with the experimental values of temperature T and normal-state resistance R_N and with the gap parameter (here and in all the following) $\Delta = 0.72$ meV.[23] The BTK parameter Z was adjusted to obtain the experimental zero-bias conductance. Samples indicating nonideal behavior by deviating, in the low-current state, too much[24] from the BTK prediction were excluded from further consideration.

Our main interest is in the high-current state. In Fig. 4 the high-current branch of the differential conductance is represented not only for the junction of Fig. 3 [sample (a)] but for two more low-resistance junctions. The ordinate $G_{norm} = G_S(U)/G_N(U)$ is normalized to the differential conductance $G_N(U)$ in the normal state. The diagram may serve to indicate the degree of reproducibility from sample to sample. Resistance values are given in the figure caption.

We have indicated pronounced minima in Fig. 4 by arrows and we associate these minima consecutively with a bubble radius (in units of ξ') $\rho = R/\xi' = 1,2,3,\ldots$. Let the voltage values corresponding to these minima be $U_1, U_2, U_3, \ldots$. Then the experimental result of Fig. 4 yields the rule of growing $\rho(U)$ of the bubble radius with voltage for samples of given resistance, at least on some discrete points. If we attribute the maxima between the minima to half-integer values of ρ, the number of points is somewhat enhanced for which $\rho(U)$ is experimentally determined. The corresponding diagram u vs ρ resulting for samples (a) and (b) is represented in Fig. 5. Here and in the following

$$u = eU/\Delta \tag{8}$$

is the voltage normalized to the gap voltage.

Normal-state resistances for samples (a) and (b) are equal, namely, $R_N = 0.29\ \Omega$. Hence, Fig. 5 represents the experimentally determined rule of growing of the nonequilibrium bubble below a 0.29 Ω contact [with differences between (a) and (b) indicating the degree of reproducibility]. Note that this resistance value is the smallest one realized by our preparation procedure. The dashed line in Fig. 5 is obtained from Eqs. (5)–(7) and represents the radii for which the local temperature should have fallen off to T_c according to Refs. 17 and 18. Note again that these radii are too small by a factor of about 6.

Figure 5 represents one of two results which have to be explained in the following sections. The second result to be explained is the dependence on contact resistance to be presented in the following.

For junctions with resistance R_N larger than those represented in Fig. 4 the minima are shifted to higher voltage. This is reasonable since one might expect the heating power U^2/R_N to remain approximately constant for a given bubble radius to be obtained. At the same time, there are only two minima observable in $G(U)$ corresponding to $\rho = 1$ and $\rho = 2$. This is due to the deviations in $G(U)$ from the normal-state conductance quickly decreasing with increasing eU/Δ. Thus finer details are not resolved in the characteristics for higher bias.

In Fig. 6 we have plotted for all our samples the position on voltage scale of the first and second minima versus contact resistance R_N. The dashed lines again are obtained from Eqs. (5)–(7). According to this latter estimate the (large) radii $\rho = 1$ and $\rho = 2$ are expected (for the applied voltage range) for resistance values much smaller than observed, i.e., for much higher heating power U^2/R_N. Thus, while Fig. 5 represents the growing law of the bubble for the smallest contact resistance, Fig. 6 contains all available experimental information concerning the dependence of bubble growing on contact resistance. The main aim of the present investigation is to understand Figs. 5 and 6.

III. MODELING THE BUBBLE GROWTH

A. Conception of the model

In the following we propose a model for the electron and phonon nonequilibrium distributions which are established in the bubble on account of multiple inelastic scattering processes of the injected electrons. The scattering is due to the electron-phonon interaction and the scattering probabilities are characterized by the Eliashberg function $\alpha^2F(\omega)$.

With the bias voltage given and a particular bubble size arbitrarily assumed we may, by simplified Boltzmann equations, calculate stationary distributions for electron and phonon excitations, $f(\vec{r},\vec{k})$ and $n(\vec{r},\vec{q})$, respectively. As usual, the distribution functions are assumed to depend on wave vectors $\vec{k}$ and $\vec{q}$ only via the quasiparticle energies ϵ and ω. Moreover, the spatial $(\vec{r})$ dependence within the bubble is replaced by mean values over the bubble. Hence we work with energy-dependent mean occupation probabilities $f(\epsilon)$ and $n(\omega)$ in the bubble. The distributions outside the bubble do not explicitly enter the model.

For given bias voltage and different bubble sizes arbitrarily assumed, quasiparticle excitation $f(\epsilon)$ will be low for large and will be high for small bubble size. If we tentatively describe the quasiparticle excitation by an effective temperature, this temperature would be low, say small compared with the critical temperature T_c, for large bubble size and would be large compared with T_c for small bubble size. Neither of both cases would be stable. Instead, too large a bubble must be expected to shrink and too small a bubble must be expected to grow. Obviously, there must be an intermediate bubble size which is stable for the given injection

bias. This bubble size in its dependence on voltage represents the growing law $\rho(u)$ we are looking for.

If the quasiparticle distribution would be thermal, $\rho(u)$ would be determined by postulating the effective temperature to equal T_c. Since it will turn out to be not, this postulate must be replaced by another suited condition. In fact, we shall postulate the (nonthermal) stationary quasiparticle distribution function $f(\epsilon)$ to satisfy the BCS gap equation for vanishing order parameter. The corresponding self-consistency equation will be given in Sec. III D below.

The quasiparticle spectra within the bubble are assumed to be given by the normal-state bulk densities of states: namely, N_0, the one-spin density of states at the Fermi level, and the energy-dependent phonon density of states, $F(\omega)$. At first sight, the use of bulk properties to describe the spectrum of excited states might seem questionable in particular for the electronic system. Remember that the finite size of the bubble leads to the quantization phenomena displayed in Fig. 1. However, from Fig. 1 we may realize that the quantization phenomena do not lead to an order of magnitude deviation from the bulk value for values of ρ between 1 and 3. Instead, the mean density of states in the subgap regime is modified only by 20%–60%. Thus, while in principle the proposed model is suited to determine $\rho(u)$ for $\rho \gg 1$ it may be expected to be not too bad in the experimentally observed range of ρ values from 1 to 3.

B. Explicit formulation of the stationarity conditions

In the following ϵ and ω are defined as dimensionless quantities: namely, the corresponding electron and phonon energies divided by the gap energy. The densities of states, however, retain their usual normalization. Hence $N_0 \Delta d\epsilon$ and $F(\omega)\Delta d\omega$ are the increments of the numbers of electronic and phononic states per unit volume.

We denote with $f(\epsilon)$ and $1-f(\epsilon)$ the mean electron and hole occupation numbers with excitation energies $\epsilon > 0$ and $-\epsilon > 0$, respectively. $n(\omega)$ was defined as the mean occupation number for phonon states with energy ω. Both, $f(\epsilon)$ and $n(\omega)$ must be stationary under the condition of given ρ and u. Thus we must have for a particular energy

$$\left(\frac{df(\epsilon)}{dt}\right)_{inj} + \left(\frac{df(\epsilon)}{dt}\right)_{esc} + \left(\frac{df(\epsilon)}{dt}\right)_{scatt} = 0 \tag{9}$$

and

$$\left(\frac{dn(\omega)}{dt}\right)_{esc} + \left(\frac{dn(\omega)}{dt}\right)_{scatt} = 0. \tag{10}$$

Here ''inj'' means ''on account of quasiparticle injection from the contact'' and ''esc'' means ''on account of quasiparticle escape from the bubble.'' The last terms on the left-hand sides of the Boltzmann equations (9) and (10) describe the effect of electron-phonon scattering and will be further discussed below.

Let us assume throughout the following that the normal side of the contact is biased negatively. Then electronlike quasiparticles are injected into the bubble. Above the gap, i.e., for $\epsilon > 1$, the occupation is very small compared with unity while $f(\epsilon)$ is very close to unity for $\epsilon < -1$, even in the high-current state. We may anticipate this from our later results on the nonequilibrium distribution function. Hence quasiparticle injection may be neglected for $\epsilon < -1$.

For $1 < \epsilon < u$ we may obtain the injection term in Eq. (9) from

$$2N_0 \left(\frac{df(\epsilon)}{dt}\right)_{inj} \frac{2\pi}{3} \xi'^3 \rho^3 \Delta d\epsilon = \frac{\Delta d\epsilon / e}{R_N} \frac{1}{e} \tag{11}$$

as

$$\left(\frac{df(\epsilon)}{dt}\right)_{inj} = \frac{(3/4\pi)}{R_N e^2 \xi'^3 \rho^3 N_0} \quad \text{for} \quad 1 < \epsilon < eU/\Delta. \tag{12}$$

To justify Eq. (11) note that the left-hand side is the increment of the number of electrons in the bubble per unit time and per energy increment $\Delta d\epsilon$. With R_N the contact resistance, the right-hand side is the corresponding injection current contribution in units of electrons per unit time.

For $|\epsilon| < 1$, quasiparticle injection may be neglected for the following reason: Any injected electronlike quasiparticle will, with high probability, elastically be Andreev reflected as a hole back through the injection orifice thus leading to no net yield of quasiparticle density in the bubble. Of course there is a finite electron and hole density within the bubble on account of this injection and elastic backscattering process. However, its contribution to the mean occupation probability $f(|\epsilon| < 1)$ is of order of magnitude $a^2/R^2 \ll 1$ and thus is negligible compared with the subgap excitation resulting from inelastic downscattering of high-energy quasiparticles into subgap states. Hence Eq. (12) may be completed by

$$\left(\frac{df(\epsilon)}{dt}\right)_{inj} = 0 \quad \text{for} \quad \epsilon > u \quad \text{and} \quad \epsilon < 1. \tag{13}$$

For the escape term in Eq. (9) we make the simplest possible assumption: namely,

$$\left(\frac{df(\epsilon)}{dt}\right)_{esc} = \begin{cases} -f(\epsilon)\dfrac{v_F}{\rho\xi'} & \text{for } \epsilon > 1, \\ 0 & \text{for } |\epsilon| < 1, \\ [1-f(\epsilon)]\dfrac{v_F}{\rho\xi'} & \text{for } \epsilon < -1. \end{cases} \tag{14}$$

For $|\epsilon| < 1$ this describes the effect of Andreev reflection preventing quasiparticles to leave the bubble. For $|\epsilon| > 1$, Eq. (14) corresponds to a mean traveling time R/v_F of an electron or hole moving a typical distance $R = \rho\xi'$ with Fermi velocity to leave the bubble.

For $|\epsilon| > 1$ the third term in Eq. (9) may be written as

$$\left(\frac{df(\epsilon)}{dt}\right)_{scatt} = \left(\frac{df(\epsilon)}{dt}\right)_{e^+} + \left(\frac{df(\epsilon)}{dt}\right)_{e^-} + \left(\frac{df(\epsilon)}{dt}\right)_{a^+} + \left(\frac{df(\epsilon)}{dt}\right)_{a^-}, \quad \text{with} \tag{15}$$

$$\left(\frac{df(\epsilon)}{dt}\right)_{e^+} = \frac{2\pi\Delta}{\hbar}[1-f(\epsilon)]\int_0^\infty f(\epsilon+\omega)\alpha^2F(\omega)[n(\omega)+1]d\omega = A_1(\epsilon), \tag{16}$$

$$\left(\frac{df(\epsilon)}{dt}\right)_{e^-} = -\frac{2\pi\Delta}{\hbar}f(\epsilon)\int_0^\infty [1-f(\epsilon-\omega)]\alpha^2F(\omega)[n(\omega)+1]d\omega = A_2(\epsilon), \tag{17}$$

$$\left(\frac{df(\epsilon)}{dt}\right)_{a^+} = \frac{2\pi\Delta}{\hbar}[1-f(\epsilon)]\int_0^\infty f(\epsilon-\omega)\alpha^2F(\omega)n(\omega)d\omega = A_3(\epsilon), \tag{18}$$

$$\left(\frac{df(\epsilon)}{dt}\right)_{a^-} = -\frac{2\pi\Delta}{\hbar}f(\epsilon)\int_0^\infty [1-f(\epsilon+\omega)]\alpha^2F(\omega)n(\omega)d\omega = A_4(\epsilon). \tag{19}$$

The symbols $A_i(\epsilon)$ are introduced as abbreviations for the right-hand sides of the above equations for later use. The subscripts e^{+-} and a^{+-} stand for phonon emission (e) or absorption (a) processes increasing ($+$) or decreasing ($-$) the occupation number $f(\epsilon)$, respectively. Equations (15)–(19) are standard results of time-dependent perturbation theory and may, e.g., be obtained from Eq. (4.35) of Ref. 25.

As they stand, Eqs. (15)–(19) hold for $|\epsilon|>1$. For $|\epsilon|<1$ these equations need some modification. We have to take into account Andreev reflection from the N/S boundary which not only prevents escape but, moreover, guarantees that electron and hole occupation numbers are equal, hence $f(\epsilon)=1-f(-\epsilon)$.

For example, think of a phonon emission process producing a subgap electron $0<\epsilon<1$. By the following elastic Andreev reflection process the electron excitation vanishes from the bubble and a hole excitation appears with the same excitation energy, i.e., with $\epsilon_{hole}=-\epsilon$ according to our convention at the beginning of this subsection. By the following Andreev reflection the hole is reconverted into an electron and so on. As a result, the phonon emission process under question has not produced an electron with unity probability but an electron and a hole, both with probability one-half. Both $f(\epsilon)$ and $1-f(-\epsilon)$ are therefore enhanced by phonon emission processes with final-state electron energy $\epsilon>0$, the corresponding value of $df(\epsilon)/dt=d[1-f(-\epsilon)]/dt$ being given by the right-hand side of Eq. (16) times one-half.

The corresponding coupling of electron and hole states does not only apply for phonon emission processes enhancing $f(\epsilon)$ for $0<\epsilon<1$ but also for absorption processes and for both types of processes decreasing $f(\epsilon)$. Moreover, also processes with negative instead of positive subgap values of ϵ as initial or final electronic state lead to contributions to $df(\epsilon)/dt$. The final result for

$$\left(\frac{df(\epsilon)}{dt}\right)_{scatt} = \left(\frac{d[1-f(-\epsilon)]}{dt}\right)_{scatt} = -\left(\frac{df(-\epsilon)}{dt}\right)_{scatt} \tag{20}$$

may be written with the aid of the abbreviations $A_i(\epsilon)$ introduced above as

$$\left(\frac{df(\epsilon)}{dt}\right)_{scatt} = \frac{1}{2}\left(\sum_{i=1}^{4} A_i(\epsilon) - \sum_{i=1}^{4} A_i(-\epsilon)\right) \quad \text{for} \quad |\epsilon|<1, \tag{21}$$

holding for either sign of ϵ and obviously satisfying Eq. (20).

The stationary phonon occupation is determined by Eq. (10). Here we set, analogously to Eq. (14),

$$\left(\frac{dn(\omega)}{dt}\right)_{esc} = -n(\omega)\frac{v_{ph}}{R}, \tag{22}$$

where v_{ph} denotes a typical phonon group velocity. We shall see later on that phonon escape is rather unimportant on account of small values of v_{ph}. Hence this ansatz is less critical than the electron escape term (14).

Electron-phonon scattering leads to

$$\left(\frac{dn(\omega)}{dt}\right)_{scatt} = \left(\frac{dn(\omega)}{dt}\right)_e + \left(\frac{dn(\omega)}{dt}\right)_a, \tag{23}$$

with the emission (e) and absorption (a) terms given by

$$\left(\frac{dn(\omega)}{dt}\right)_e = 2N_0\frac{2\pi\Delta}{\hbar}\alpha^2(\omega)[1+n(\omega)] \times \int_{-\infty}^{+\infty}[1-f(\epsilon-\omega)]f(\epsilon)d\epsilon = B_1(\omega) \tag{24}$$

and

$$\left(\frac{dn(\omega)}{dt}\right)_a = -2N_0\frac{2\pi\Delta}{\hbar}\alpha^2(\omega)n(\omega) \times \int_{-\infty}^{+\infty} f(\epsilon)[1-f(\epsilon+\omega)]d\epsilon = B_2(\omega), \tag{25}$$

respectively. Equation (24) may be made obvious from Eq. (17) which implies that the number of phonons from the interval $(\omega,\omega+d\omega)$ produced per unit time and per unit vol-

ume by phonon emission processes with initial electron energy between ϵ and $\epsilon+d\epsilon$ is given by

$$2N_0\Delta d\epsilon\frac{2\pi\Delta}{\hbar}f(\epsilon)[1-f(\epsilon-\omega)][n(\omega)+1]\alpha^2F(\omega)d\omega.$$

Integrated over ϵ this must be equal to the total number of phonons emitted per unit time and per unit volume in the interval $(\omega,\omega+d\omega)$: namely,

$$F(\omega)\Delta d\omega\left(\frac{dn(\omega)}{dt}\right)_e.$$

The corresponding equation is just Eq. (24). Equation (25) is made obvious in a similar manner.

C. Algorithm, compilation of formulas

We have now at our disposal all equations which are needed to determine the stationary distributions $f(\epsilon)$ and $n(\omega)$ for given injection bias and given bubble radius $R=\rho\xi'$. We summarize these equations in a form suited for a numeric algorithm.

Inserting Eqs. (12), (13), (14), (15) [or, alternatively, Eq. (21)], and finally Eqs. (16), (17), (18), and (19) into Eq. (9) and, moreover, inserting Eqs. (22)–(25) into Eq. (10), we obtain two equations which may be written as

$$F_1+f(\epsilon)G_1=0 \tag{26}$$

and

$$F_2+n(\omega)G_2=0, \tag{27}$$

with

$$F_1=J_{inj}+J^{(F)}_{esc,el}+J_{11}, \tag{28}$$

$$G_1=J^{(G)}_{esc,el}-J_{11}+J_{12}, \tag{29}$$

$$F_2=N_0\frac{4\pi\Delta}{\hbar}\alpha^2(\omega)\int_{-\infty}^{+\infty}[1-f(\epsilon-\omega)]f(\epsilon)d\epsilon, \tag{30}$$

$$G_2=J_{esc,ph}+J_2. \tag{31}$$

Here the following abbreviations are used:

$$J_{inj}=\begin{cases}\left[\frac{4\pi}{3}R_Ne^2\xi'^3\rho^3N_0\right]^{-1} & \text{for} \quad 1<\epsilon<u,\\ 0 & \text{otherwise}\end{cases} \tag{32}$$

$$J^{(F)}_{esc,el}=\frac{v_F}{\rho\xi'}\times\begin{cases}0 & \text{for} \quad \epsilon>-1,\\ 1 & \text{for} \quad \epsilon<-1,\end{cases} \tag{33}$$

$$J^{(G)}_{esc,el}=-\frac{v_F}{\rho\xi'}\times\begin{cases}1 & \text{for} \quad |\epsilon|>1,\\ 0 & \text{for} \quad |\epsilon|<1,\end{cases} \tag{34}$$

$$J_{11}=\frac{2\pi\Delta}{\hbar}\times\begin{cases}\int_0^\infty\alpha^2F(\omega)\{f(\epsilon+\omega)[n(\omega)+1]+f(\epsilon-\omega)n(\omega)\}d\omega & \text{for} \quad |\epsilon|\geqslant1,\\ \int_0^\infty\alpha^2F(\omega)\left\{\frac{1}{2}[f(\epsilon+\omega)-f(-\epsilon+\omega)][n(\omega)+1]\right.\\ \qquad\left.+\frac{1}{2}[f(\epsilon-\omega)-f(-\epsilon-\omega)]n(\omega)\right\}d\omega & \text{for} \quad |\epsilon|<1,\end{cases} \tag{35}$$

$$J_{12}=-\frac{2\pi\Delta}{\hbar}\times\begin{cases}\int_0^\infty\alpha^2F(\omega)\{[1-f(\epsilon-\omega)][n(\omega)+1]+[1-f(\epsilon+\omega)]n(\omega)\}d\omega & \text{for} \quad |\epsilon|\geqslant1,\\ \int_0^\infty\alpha^2F(\omega)\left\{\frac{1}{2}[f(-\epsilon-\omega)-f(\epsilon-\omega)][n(\omega)+1]\right.\\ \qquad\left.+\frac{1}{2}[f(-\epsilon+\omega)-f(\epsilon+\omega)]n(\omega)\right\}d\omega & \text{for} \quad |\epsilon|<1,\end{cases} \tag{36}$$

$$J_{esc,ph}=-\frac{v_{ph}}{\rho\xi'}, \tag{37}$$

$$J_2=N_0\frac{4\pi\Delta}{\hbar}\alpha^2(\omega)\int_{-\infty}^{+\infty}[f(\epsilon+\omega)-f(\epsilon-\omega)]f(\epsilon)d\epsilon. \tag{38}$$

Note that the quantities F_1 and G_1 depend on ϵ and, moreover, are functionals of the distributions to be determined: namely, $f(\epsilon')$ and $n(\omega)$. Similarly, F_2 and G_2 depend on ω and are functionals of $f(\epsilon')$. This will be indicated by the notation below. All other quantities entering the above equations are known experimental data for tantalum and will be given in Sec. IV.

Equations (26) and (27) may be written as

$$f(\epsilon) = -\frac{F_1[\epsilon, f(\epsilon'), n(\omega)]}{G_1[\epsilon, f(\epsilon'), n(\omega)]}, \tag{39}$$

$$n(\omega) = -\frac{F_2[\omega, f(\epsilon')]}{G_2[\omega, f(\epsilon')]}, \tag{40}$$

and in this form represent the basis for an iterative numerical algorithm to determine the distribution functions $f(\epsilon)$ and $n(\omega)$ by the following steps.

(i) Assume a suited initial quasiparticle distribution $f_0(\epsilon')$.

(ii) From this calculate an initial phonon distribution $n_0(\omega)$ using Eq. (40).

(iii) Insert these starting functions $f_0(\epsilon')$ and $n_0(\omega)$ on the right-hand side of Eq. (39) to obtain a better $f(\epsilon)$, say $f_1(\epsilon)$.

(iv) With $f_1(\epsilon')$ inserted into Eq. (40) obtain $n_1(\omega)$.

(v) Repeat steps (iii) and (iv) to obtain $f_\nu(\epsilon)$, $n_\nu(\omega)$ as results of the νth iteration. Continue until $f_\nu(\epsilon)$ equals $f_{\nu-1}(\epsilon)$ with sufficient precision.

This iteration procedure converged after a few iterations yielding $f(\epsilon)$ and $n(\omega)$ for given injection bias voltage U and given bubble radius ρ. Results will be given in Sec. V.

D. Self-consistency equation

The above-sketched numerical program leads to distribution functions $f(\epsilon)$ and $n(\omega)$ for any assumed pair of u and ρ values. However, for given u only one particular value of ρ will be established corresponding to an electronic excitation $f(\epsilon)$ just necessary to destroy superconductivity. We obtain the corresponding condition for $f(\epsilon)$ from the BCS gap equation[26] for vanishing gap parameter: namely,

$$1 = N_0 V \int_0^{\hbar\omega_D/\Delta} \frac{1-2f(\epsilon)}{\epsilon} d\epsilon. \tag{41}$$

If $f(\epsilon)$ were the Fermi function for temperature T_c, Eq. (41) would determine T_c with the well-known result $kT_c = 0.568\Delta$. For the real nonequilibrium case we shall determine, for a given ρ, that particular U which just produces a nonequilibrium distribution $f(\epsilon)$ satisfying Eq. (41). It is obvious that the corresponding numerical program will lead to a unique value of U since $f(\epsilon)$ must, for any ϵ, be expected monotonically to increase with U and hence the right-hand side of Eq. (41) will monotonically decrease.

Using the BCS result $\ln(2\hbar\omega_D/\Delta) = (N_0 V)^{-1}$, which is a good approximation for $\hbar\omega_D \gg \Delta$, Eq. (41) may be brought to the form

$$\int_0^1 \frac{1-2f(\epsilon)}{\epsilon} d\epsilon - 2\int_1^{\hbar\omega_D/\Delta} \frac{f(\epsilon)}{\epsilon} d\epsilon - \ln 2 = 0. \tag{42}$$

Using Eq. (41) as a starting point we have assumed particle-hole symmetry $f(\epsilon) = 1 - f(-\epsilon)$. While this condition is granted by our model for $|\epsilon| < 1$ we shall see later on that it is violated for $|\epsilon| > 1$. However, we shall also find from the numerical data that the second contribution in Eq. (42) will be negligibly small and thus the same is true for the error made by assuming particle-hole symmetry. In fact, Eq. (42) may well be replaced by

$$L(u) := \int_0^1 \frac{1-2f(\epsilon)}{\epsilon} d\epsilon - \ln 2 = 0, \tag{43}$$

which is the final form of the self-consistency condition to be applied in the following. The symbol $L(u)$ is introduced for later use.

IV. ELECTRON AND PHONON PROPERTIES OF TANTALUM

A. Constants entering the model

To apply the above-described model we need an independently known set of data for tantalum. The model being coarse grained enough we want to avoid any adjusting of parameters and instead to take all necessary data from the literature. Before discussing our knowledge of the Eliashberg function $\alpha^2F(\omega)$ we shortly summarize our choice of the parameters N_0, Δ, v_F, ξ', and v_{ph} entering the model. We assume the following values:

$\Delta = 0.72$ meV (Ref. 23),

$2\xi'/\pi^2 = \xi_0 = 92.5$ nm (Ref. 27),

$N_0 = 2.04 \times 10^{47} \mathrm{J}^{-1}\mathrm{m}^{-3}$ (Ref. 28),

$v_F = 3.18 \times 10^5$ m/s.

v_F was deduced from the well-established experimental data for Δ and ξ_0 using the BCS relation $\xi_0 = \hbar v_F/(\pi\Delta)$. Hence the data for Δ, ξ_0, and v_F are consistent. Finally, the phonon group velocity strongly depends on phonon branch index and frequency. Maximum values are obtained in the long-wavelength limit. From the elastic constants given by Featherston and Neighbors[29] one obtains about 2000 m/s for transverse and about double this value for longitudinal phonons. These values are small enough to neglect phonon escape completely in our model setting $v_{ph} = 0$. We shall demonstrate this later on by a few examples comparing results for $v_{ph} = 0$ or 2000 m/s, respectively.

B. Eliashberg function

In principle, the formulas given in Sec. III C contain both, the Eliashberg function $\alpha^2F(\omega)$ and $\alpha^2(\omega)$, the average squared electron-phonon interaction matrix element. However, with $\alpha^2F(\omega)$ being given, the final results for the stationary distributions $f(\epsilon)$ and $n(\omega)$ are practically independent of $\alpha^2(\omega)$. This is true because phonon escape may be neglected, as was stated before. That $\alpha^2(\omega)$ does not enter the model results for $v_{ph} = 0$ is most easily seen by inspecting Eqs. (39) and (40) and the preceding formulas defining the symbols entering these equations. For $v_{ph} = 0$, F_2 and G_2 are both proportional to $\alpha^2(\omega)$ and hence $n(\omega)$ is independent of $\alpha^2(\omega)$ according to Eq. (40). Finally, $f(\epsilon)$ as given by Eq. (39) does not depend on $\alpha^2(\omega)$ since $n(\omega)$ does not.

The Eliashberg function for tantalum was determined from N/S tunneling data by Shen.[23] Very similar results have later on been reported by other authors.[30–32] Shen's experi-

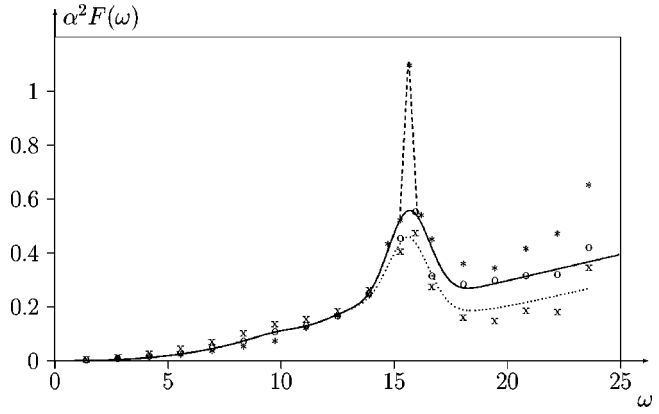

FIG. 7. Eliashberg function $\alpha^2F(\omega)$ as determined by Shen (Ref. 23) (o), Wolf *et al.* (Ref. 32) (x), and Al-Lehaibi *et al.* (Ref. 28) (*). Solid line: analytical interpolation of Shen's data. Dashed and dotted lines: variants.

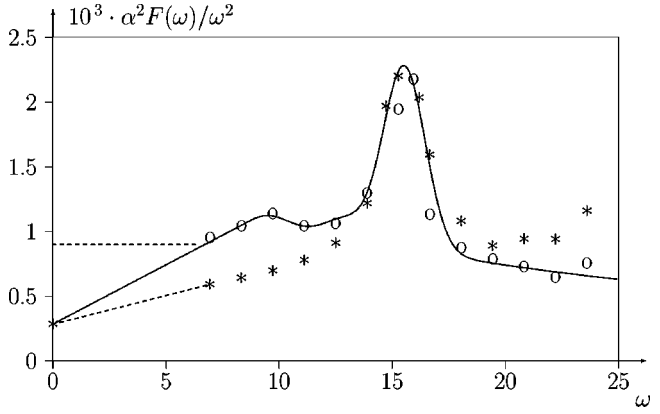

FIG. 8. $\alpha^2F(\omega)/\omega^2$ vs ω. Data (o), (*) and solid line taken from Fig. 7. Dashed lines: see text.

mental result, represented by circles in Fig. 7, is well represented by the solid line in the same diagram. This interpolating line will be used for all of the following calculations. It corresponds to an ad-hoc analytical expression which however, need not be given here since there is no physical reasoning behind it and since the interpolation may, with sufficient precision, be obtained from Fig. 8 below. Fig. 7 also contains the α^2F-data obtained from tunneling experiments by Wolf et al.[32] and the data calculated theoretically by Al-Lehaibi, Swihart, Butler, and Pinski.[28] $\alpha^2F(\omega)$ is needed only for energies below $\omega \approx 25$ corresponding to the maximum values of eU/Δ appearing in the experiments (see Fig. 6). As a consequence, only the transverse phonon peak is represented in Fig. 7, the longitudinal phonon peak of the characteristic double peak structure lying at somewhat higher energies.

The model results are rather insensitive to modifications of $\alpha^2F(\omega)$ in the range $\omega > 10$. For example, calculations based on the dashed or dotted instead of the solid curve in Fig. 7 yield maximum deviations in the calculated $\rho(u)$ of less than 0.5% which are negligible. On the other hand, for low energies, say up to several times the gap energy, reliable values for $\alpha^2F(\omega)$ are not available from tunneling. This is due to the extremely small values of $\alpha^2F(\omega)$ in this regime leading to error bars of 100% order of magnitude. A method of nevertheless plotting $\alpha^2F(\omega)$ down to $\omega = 0$ is to simply assume a behavior proportional ω^2, i.e.,

$$\alpha^2F(\omega) = b\omega^2 \tag{44}$$

below some low-lying energy. Thus in Ref. 30 a corresponding assumption was made for energies below 5 meV, corresponding to $\omega \approx 7$. Shen's data handling obviously was performed in the same way with the result of $b = 0.9$.[33,34] Nevertheless, the tunneling results must, for general methodical reasons, be considered as principally unknown for energies up to a few times the gap energy. This uncertainty is rather unimportant with respect to the superconducting equilibrium properties onto which interest was focused in the papers quoted above. However, the results of the present investigation strongly depend on the low-energy behavior of $\alpha^2F(\omega)$.

Fortunately, the theoretical data of Ref. 28 allow for an improved extrapolation to the low energy regime. From Fig. 1 of Ref. 28 we obtain $\alpha^2(\omega)$ which (some small spurious oscillations neglected) varies roughly linearly from 2.7×10^{-51} J m^3 at very low energies to 6×10^{-51} J m^3 at $\omega = E/\Delta \approx 20$.[35] The former value allows to estimate $\alpha^2F(\omega)/\omega^2$ for very low energies since $F(\omega)/\omega^2$ may be obtained from the elastic constants which were determined for tantalum by Featherston and Neighbors[29]. From their data we obtain (omitting details of the estimate) $\lim_{\omega \to 0}[F(\omega)/\omega^2] = 1.04 \times 10^{47}$ J^{-1}m^{-3}. With $\alpha^2 = 2.7 \times 10^{-51}$ J m^3 we finally have

$$\lim_{\omega \to 0}[\alpha^2F(\omega)/\omega^2] = 0.28 \times 10^{-3}. \tag{45}$$

Figure 8 shows $\alpha^2(\omega)/\omega^2$ vs ω. The theoretical data of Ref. 28 are again represented by stars and by the value at $\omega = 0$ given above. Shen's data (represented by circles) may be linearly extrapolated to this value. We claim this extrapolation to be more reliable than the quadratic extrapolation to the above-given value $b = 0.9$ (the latter extrapolation is indicated by the dashed horizontal line).

The remaining difference between the data by Shen and by Al-Lehaibi *et al.* is due to the fact that the theoretical calculation does not yield the extra structure at 7 mV (or ω slightly below 10) which is, however, well established by the tunneling data from different authors. Hence, the solid line in Figs. 7 and 8 will be used to represent the Eliashberg function in all of the following calculations.

V. MODEL RESULTS

In the following we present typical results. The ϵ and ω scales were divided into finite intervals of length $\delta\epsilon = \delta\omega$ and the integrations of Sec. III C were replaced by summations over these intervals with a suited cutoff. $\delta\epsilon = \delta\omega = 0.1$ was chosen since choosing smaller intervals did practically not alter the results. The iteration procedure practi-

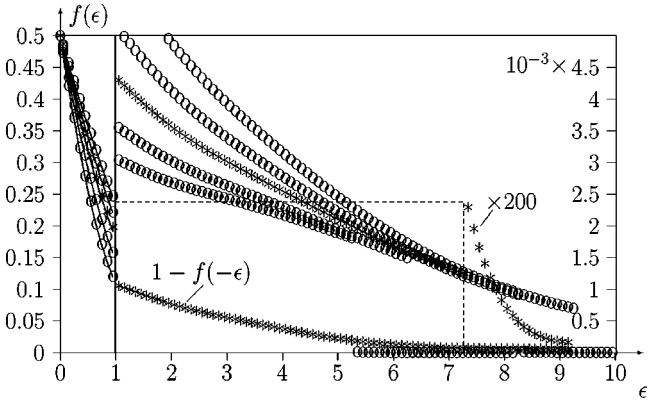

FIG. 9. Distribution function $f(\epsilon)$ for $R_N=0.29\ \Omega$, $\rho=1$, and (from top to bottom) $u=9.28$, 8.28, 7.28, 6.28, and 5.28, respectively. Left-hand and right-hand ordinate scales valid for $\epsilon<1$ and $|\epsilon|>1$, respectively. For $u=7.28$ (symbol *) the self-consistency equation is satisfied. For this u value also the hole excitation $1-f(-\epsilon)$ is represented. Dashed line: see Ref. 36.

cally converged after three or four iterations with a precision given by the linewidth of the following graphical presentation of results. Actually, six iterations were applied in all cases.

Figure 9 represents, as an example, electronic quasiparticle distributions for the parameters $R_N=0.29\ \Omega$, $\rho=1$ (i.e., $R=\xi'$), and five different voltage values given in the figure caption. The figure demonstrates the main features of all of our results: Excitation is high for subgap states and is two orders of magnitude lower for $1<\epsilon<u$ and for $\epsilon<-1$ (note the different scaling for sub-gap and above-gap energies, respectively). The reason for this behavior was outlined above: Quasiparticles excited above the gap quickly escape, leading to a low mean occupation within the normal half-sphere, while subgap quasiparticles cannot escape because they are Andreev reflected.[36]

For $\epsilon>u$, there is no injection and excitation is unmeasurably small on the right-hand scale of Fig. 9. For one of the five curves (corresponding to $u=7.28$) $f(\epsilon)$ is displayed in this region enlarged by a factor of 200. For the same voltage parameter the hole excitation $1-f(-\epsilon)$ is also displayed for $\epsilon>1$. For $0<\epsilon<1$ the hole excitation $1-f(-\epsilon)$ equals $f(\epsilon)$ as displayed in the figure and hence does not need to be displayed separately.

For given R_N and ρ, the distribution functions $f(\epsilon)$ and $n(\omega)$ were calculated for varying voltage u. In each case the left-hand side of the self-consistency equation (43), $L(u)$, was calculated. As outlined before, $L(u)$ monotonically decreases with u. We determined by interpolation that value of u for which $L(u)$ vanishes; i.e., the self-consistency equation is satisfied. This is just the voltage corresponding to the given values of R_N and ρ and thus constitutes the result of the theoretical model. Figure 9 just represents some typical results for the parameters $R_N=0.29\ \Omega$ and $\rho=1$. The value $u=7.28$ corresponding to the middle one of the five curves was obtained by interpolation as that value for which $L(u)$ practically vanishes. We have, with an error of less than 0.005,

$$L(5.28)=0.249,\quad L(6.28)=0.113,\quad L(7.28)=0.004,$$

$$L(8.28)=-0.082,\quad L(9.28)=-0.151.$$

The u values satisfying $L(u)=0$ were calculated for varying values of contact resistance R_N and bubble radius ρ. In Figs. 5 and 6 the results are shown and compared with the experimental results. The solid lines represent the results for $v_{ph}=0$ which, according to Sec. IV B, depend on $\alpha^2F(\omega)$ only and not [with $\alpha^2F(\omega)$ given] on $\alpha^2(\omega)$ and $F(\omega)$ separately. The dotted and dash-dotted curves were calculated with $v_{ph}=2000$ m/s, $\alpha^2F(\omega)$ as given and assuming α^2 independent of ω and equal to 6×10^{-51} J m^3 and 2.7×10^{-51} J m^3, respectively. Remember these being the extremal α^2 values according to Sec. IV B. As stated before, the differences between solid, dotted, and dash-dotted curves are unimportant proving that phonon escape may be neglected.

On the whole, Figs. 5 and 6 show that the model is well suited to explain the growing of the normal bubble within the limits of experimental reproducibility and of restricted knowledge of the Eliashberg function. In particular, progress in understanding is obvious if we compare the calculated curves with the predictions of Ref. 17 represented by the dashed curves in Figs. 5 and 6.

VI. DISCUSSION

Figures 5 and 6 constitute the most important result of this paper by proving that the scale of the experimentally observed growing of bubble size with injection is very close to what is theoretically expected. To obtain such an understanding has been the main purpose of the present investigation. As we have seen, the nonequilibrium structure is governed by Andreev reflection, preventing escape of subgap quasiparticles and thus leading to high occupation of subgap states even in a large volume. We emphasize that such an effect, while seeming natural for the N/S structure under question, is not to be expected for a weak link (w) between two superconductors, say an S/w/S structure with an electric field across "w." In the latter case any subgap quasiparticle, Andreev reflected between both S banks, would quickly escape from the w region by the effect of acceleration in the field as described, e.g., by Klapwijk *et al.*[37] or by Kümmel *et al.*[38] Since most of the previous investigations on hot spots (including the paper by Skocpol, Beasley, and Tinkham[39] opening the field) have been on weak-link structures between superconducting banks, the phenomenon investigated here seems not to have been observed before.

There have been some observations, by the Kharkov group,[40,41] of nonequilibrium under high-current conditions for N/S point contacts, with tantalum as the superconductor. However, there is no direct access to the spatial extend of the nonequilibrium region which in our case is obtained from the Tomasch-type oscillations. Hence there is no direct comparison possible between the results of both groups. In view of the importance of measuring the bubble size we want to emphasize that two conditions must be given (and are so with our samples) in order to observe the oscillations under ques-

tion: The mean free path must be markedly larger than ξ', and a very smooth surface is necessary. Such a surface results from our procedure of preparing the tantalum samples as molten drops in ultrahigh vacuum and not destroying this smoothness by the succeeding preparation steps. Both these conditions are usually not satisfied in point contact investigations.

A final comment concerns the remarkable simplicity of the applied model. Why does neither the electric field in the bubble nor the supercurrent in the S region influence the results? Both features are due to the large size of the bubble: The electric field essentially is confined to distances from the contact of order of magnitude of the orifice diameter $2a$. Hence nearly all of the bubble volume is practically field free — see Fig. 2. Finally, the (three-dimensional) spatial spread of the current leads, in the S region, to a current density smaller than $U/(R_N \times 2\pi R^2)$ which is easily estimated to be far below the critical current density, again due to the large values of R.

Among the remaining problems we mention the consistent description of the observed hysteresis. Moreover, one would like to avoid to use bulk properties in describing the electronic system in the bubble. Instead, a more realistic description is desirable of finite-size effects on the quasiparticle system. One might hope that such a description removes an obvious remaining systematic deviation between experiment and theory: namely, the different curvature of both in Fig 5.

ACKNOWLEDGMENTS

The authors would like to thank R. Kümmel and P. Seidel for stimulating discussions. Support to the experimental part was given by the Deutsche Forschungsgemeinschaft.

[1] P.G. de Gennes and D. Saint-James, Phys. Lett. **4**, 151 (1963).
[2] W.J. Tomasch, Phys. Rev. Lett. **15**, 672 (1965); **16**, 16 (1966).
[3] J.M. Rowell and W.L. McMillan, Phys. Rev. Lett. **16**, 434 (1966).
[4] A.P. van Gelder, Phys. Rev. **181**, 787 (1969).
[5] A. Hahn, Physica B **165&166**, 1065 (1990).
[6] H. Plehn, O.J. Wacker, and R. Kümmel, Phys. Rev. B **49**, 12 140 (1994).
[7] G.B. Arnold, Phys. Rev. B **18**, 1076 (1978).
[8] M. Belogolovskii, M. Grajcar, P. Kus, A. Plecenik, S. Benacka, and P. Seidel, Phys. Rev. B **59**, 9617 (1999).
[9] A. Hahn, Phys. Rev. B **31**, 2816 (1985).
[10] A. Hahn and K. Hümpfner, Phys. Rev. B **51**, 3660 (1995).
[11] A.VI. Gurewich and R.G. Mints, Rev. Mod. Phys. **59**, 941 (1987).
[12] R. Gross and D. Koelle, Rep. Prog. Phys. **57**, 651 (1994).
[13] This is in contrast with Ref. 10, where a normal full-sphere below the contact was assumed. A structure according to Fig. 2 now seems more probable. Measuring the bubble cross section according to Ref. 10 by counting the number of entering flux quanta seems nevertheless justified. However, this point is not relevant for the present investigation and hence is not further discussed here.
[14] A.F. Andreev, Zh. Eksp. Teor. Fiz. **46**, 1823 (1964) [Sov. Phys. JETP **19**, 1228 (1964)].
[15] U. Gunsenheimer and A. Hahn, Physica B **218**, 141 (1996).
[16] The solutions of the Bogoljubow–de Gennes equations in the half-sphere case are the same as those of the isolated (full) sphere, with the exception that only those are retained which vanish on the surface, i.e., those with odd quantum number $l - |m|$. These are just half of all for half of the volume. The density of states thus remains unaltered.
[17] M. Tinkham, M. Octavio, and W.J. Skocpol, J. Appl. Phys. **48**, 1311 (1977).
[18] M. Tinkham, in *Nonequilibrium Superconductivity, Phonons, and Kapitza Boundaries*, edited by K. E. Gray, Vol. 65 of *NATO Advanced Study Institute, Series B: Physics* (Plenum, New York, 1981), Chap. 8.
[19] Apex angle $2\Theta = \pi$, mean free path $l \to \infty$ [this yields an upper limit for $r(T_c)$].
[20] K. Hümpfner, Ph.D. thesis, Ruhr-Universität Bochum, 1997.
[21] The current-voltage characteristics is not shown here. A typical example may be found in Fig. 4 of Ref. 10.
[22] G.E. Blonder, M. Tinkham, and T.M. Klapwijk, Phys. Rev. B **25**, 4515 (1982).
[23] L.Y.L. Shen, Phys. Rev. Lett. **24**, 1104 (1970).
[24] The following criterion was applied: Assuming a suited constant resistance R_{Ser} in series with the contact not only the zero-bias conductance $G(U=0)$ but also $d^2G/dU^2(U=0)$ may be reproduced. If R_{Ser} exceeded 20% of R_N, the sample was excluded.
[25] A.G.M. Jansen, A.P. van Gelder, and P. Wyder, J. Phys. C **13**, 6073 (1980).
[26] P. G. de Gennes, *Superconductivity of Metals and Alloys* (Benjamin, New York, 1966), Eq. (4-125).
[27] J. Auer and H. Ullmeier, Phys. Rev. B **7**, 136 (1973).
[28] A. Al-Lehaibi, J.C. Swihart, W.H. Butler, and F.J. Pinski, Phys. Rev. B **36**, 4103 (1987).
[29] F.H. Featherston and J.R. Neighbours, Phys. Rev. **130**, 1324 (1963).
[30] K. Gärtner and A. Hahn, Z. Naturforsch. A **31**, 858 (1976).
[31] Y.F. Revenko, A.I. D'yachenko, V.M. Svistunov, and B. Shonaikh, Fiz. Nizk. Temp. **6**, 1304 (1980).
[32] E.L. Wolf, D.M. Burnell, Z.G. Khim, and R.J. Noer, J. Low Temp. Phys. **44**, 89 (1981).
[33] S.B. Kaplan, C.C. Chi, D.N. Langenberg, J.J. Chang, S. Jafarey, and D.J. Scalapino, Phys. Rev. B **14**, 4854 (1976).
[34] Table 1 of Ref. 33 contains the b value under question with reference to an unpublished paper by Rowell *et al.* which in turn is obviously based on Shen's data.
[35] The $\alpha^2(\omega)$ data are given in Rydberg units in Fig. 1 of Ref. 28 and refer to the volume of one atom. They have been recalculated to joule and m^3 units used here.
[36] The order of magnitude of the above-gap excitation may be estimated from the hypothetical case of no electron-phonon interaction at all, $\alpha^2F(\omega)=0$. Equilibrium of injection and escape would then lead, for $u=7.28$, to the energy-independent mean occupation indicated by the dashed line in Fig. 9. Electron-phonon scattering has the effect of shifting this distribution to

lower energies without altering its order of magnitude.

[37] T.M. Klapwijk, G.E. Blonder, and M. Tinkham, Physica B & C **109+110B**, 1657 (1982).

[38] R. Kümmel, U. Gunsenheimer, and R. Nicolsky, Phys. Rev. B **42**, 3992 (1990).

[39] W.J. Skocpol, M.R. Beasley, and M. Tinkham, J. Appl. Phys. **45**, 4054 (1974).

[40] I.K. Yanson, L.F. Rybal'chenko, N.L. Bobrov, and V.V. Fisun, Fiz. Nizk. Temp. **12**, 552 (1986) [Sov. J. Low Temp. Phys. **12**, 313 (1986)].

[41] I.K. Yanson, N.L. Bobrov, L.F. Rybal'chenko, and V.V. Fisun, Fiz. Nizk. Temp. **13**, 1123 (1987) [Sov. J. Low Temp. Phys. **13**, 635 (1987)].